

# Hairpin vortex organization in wall turbulence<sup>a)</sup>

Ronald J. Adrian

*Laboratory for Energetic Flow and Turbulence, Department of Mechanical and Aerospace Engineering,  
Arizona State University, Tempe, Arizona 85287*

(Received 31 October 2006; accepted 13 February 2007; published online 18 April 2007)

Coherent structures in wall turbulence transport momentum and provide a means of producing turbulent kinetic energy. Above the viscous wall layer, the hairpin vortex paradigm of Theodorsen coupled with the quasistreamwise vortex paradigm have gained considerable support from multidimensional visualization using particle image velocimetry and direct numerical simulation experiments. Hairpins can autogenerate to form packets that populate a significant fraction of the boundary layer, even at very high Reynolds numbers. The dynamics of packet formation and the ramifications of organization of coherent structures (hairpins or packets) into larger-scale structures are discussed. Evidence for a large-scale mechanism in the outer layer suggests that further organization of packets may occur on scales equal to and larger than the boundary layer thickness. © 2007 American Institute of Physics. [DOI: [10.1063/1.2717527](https://doi.org/10.1063/1.2717527)]

## I. INTRODUCTION

One of the principal schools of thought in the study of turbulence seeks to break the complex, multiscaled, random fields of turbulent motion down into more elementary organized motions that are variously called *eddies*<sup>1</sup> or *coherent structures*.<sup>2</sup> These motions can be thought of as individual entities if they persist for long times, i.e., if they possess *temporal coherence*. By virtue of fluid continuity, all motions possess some degree of spatial coherence, so coherence in space is not sufficient to define an organized motion. Only motions that live long enough to catch our eye in a flow visualization movie and/or contribute significantly to time-averaged statistics of the flow merit the study and attention we apply to organized structures. The kinematic properties of such motions (size, scaling properties, shape, vorticity, energy) and the dynamic properties (origin, stability, growth, genesis into new forms, and contribution to averages) are all of interest.

This paper is concerned with the structure of organized motion in the canonical forms of wall turbulence: steady, fully developed, incompressible, smooth-walled pipe and channel flow and the zero pressure gradient boundary layer. While these are the simplest possible wall flows, they exhibit most of the phenomena that are needed to understand turbulent flow over surfaces in more general cases. They contain Reynolds stresses that transport mean momentum, they produce and dissipate turbulent kinetic energy, and they are inhomogeneous, with lengths varying from a multiple of the viscous length scale  $\delta_v$ , near the wall to a multiple of the outer length scale  $\delta_0$  imposed by the pipe radius,  $R$ , the channel half-height,  $h$ , or the boundary layer thickness,  $\delta$ . It is believed that an understanding of the structure of coherent eddies in these flows constitutes a foundation on which to understand more complex wall flows and significantly ad-

vance the development of ideas for scaling, manipulating and controlling wall turbulence. Less practically, but perhaps more satisfactorily, understanding the forms of the eddies, their origins, and their roles in creating stress and transporting energy in these canonical flows would go far toward answering some of the most tantalizing and long-standing questions in turbulence.

To begin, it is useful to summarize briefly the essential elements of wall turbulence, mainly to establish notation and define terms. Much of what we know can be inferred from the simple observation that the effect of turbulence on the mean flow is to flatten the profile relative to the parabolic profile that occurs in pipe and channel flow or the Blasius profile that occurs in the zero-pressure gradient laminar boundary layer, Fig. 1. The total shear stress is a sum of the Reynolds shear stress  $-\rho\bar{uv}$  and the viscous stress,  $\tau(y) = -\rho\bar{uv} + \mu dU/dy$ . In fully developed pipe flow and channel flow, the absence of streamwise acceleration requires the stress to decrease linearly from the value at the wall,  $\tau_w = \tau(y=0) = \mu(dU/dy)_0$ , to zero at the centerline, where symmetry requires that  $-(\bar{uv})_{\delta_0}$  and  $(dU/dy)_{\delta_0}$  each vanish. Consequently,  $\tau(y) = \tau_w(1 - y/\delta_0)$ . (The streamwise mean velocity is  $U$ , the streamwise and wall-normal velocity fluctuations about the mean are  $u$  and  $v$ ,  $y$  is distance from the wall,  $\rho$  is density, and  $\mu$  and  $\nu = \mu/\rho$  are the dynamic and kinematic viscosity, respectively.) The flattening of the mean velocity profile implies that viscous shear stress drops below the linear variation, as sketched in Fig. 1, so that the Reynolds shear stress must start from zero at the wall, increase to a maximum at some location,  $y_p$ , and then asymptote to the linear curve as the slope of  $U(y)$  vanishes.

The net force exerted by the Reynolds shear stress is  $d(-\rho\bar{uv})/dy$ , and according to the variation of the Reynolds shear stress sketched in Fig. 1, the net force must be negative and roughly constant above  $y_p$  and positive below  $y_p$ . In this way, mean transport of turbulent momentum represented by the net Reynolds force retards the mean velocity in the core of the flow and accelerates it near the wall. The increased

<sup>a)</sup>This paper is based on the Otto Laporte Award Lecture, presented by the author at the 58th Annual American Physical Society Division of Fluid Dynamics Meeting, which was held 20–22 November 2005 in Chicago, IL.

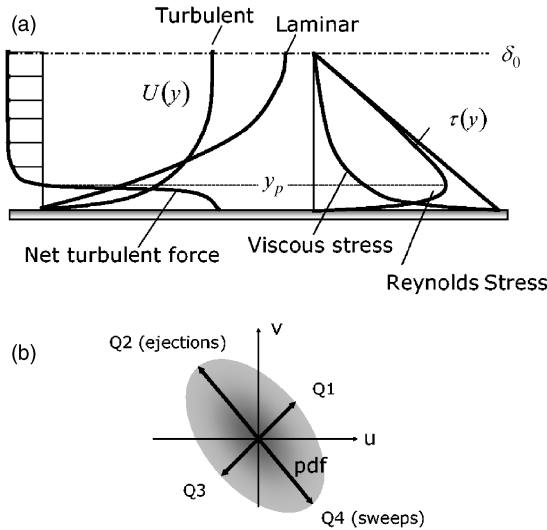


FIG. 1. Profiles of shear stresses and net force due to Reynolds shear stress  $\bar{uv}$  in fully developed pipe and channel flow. The profiles are qualitatively similar for the boundary layer. The contributions to  $-\bar{uv}$  arise from the probability density function's bias toward events in the second and fourth quadrant of the  $u$ - $v$  plane.

mean velocity near the wall causes the gradient of the mean velocity to increase, leading to higher wall shear stress.

Because of the leading role Reynolds stresses play as the first unclosed quantities in the hierarchy of Reynolds moment equations, the foremost question in wall turbulence concerns the mechanisms responsible for creating Reynolds shear stress. That is, what specific eddy motions cause the  $u$  and  $v$  components to be anticorrelated and to vary as observed? It is well known that the probability density function of the  $u$  and  $v$  fluctuations behaves qualitatively as shown in Fig. 1, with more probability of spending time in the second (Q2) and fourth (Q4) quadrants of the  $u$ - $v$  plane, so that the average of  $u$  times  $v$  is negative. Events in the second quadrant correspond to negative streamwise fluctuations being lifted away from the wall by positive wall-normal fluctuations, and they are referred to as *ejections*.<sup>3</sup> Events in the fourth quadrant correspond to positive streamwise fluctuations being moved toward the wall. They are associated with motions called *sweeps*.<sup>3,4</sup> Quadrant analysis of this type does not explain the form of the eddies creating sweeps and ejections, but it does permit evaluation of the contributions these events make to the total mean values of various quantities such as kinetic energy, dissipation, etc.

Because of the linear variation of total stress, the wall shear stress and the Reynolds shear stress are related, justifying the introduction of the *friction velocity*  $u_\tau = \sqrt{\tau_w/\rho}$  as a scale representative of the turbulent fluctuations. The viscous length scale alluded to earlier is given by  $\delta_v = v/u_\tau$ , and distance above the wall scaled in wall units is denoted by  $y^+ = y/\delta_v$ . The law of the wall states that  $U^+ \equiv U/u_\tau = g(y^+)$ , where the function  $g$  is independent of Reynolds number. The von Karman number is defined as the ratio of the outer length scale to the viscous length scale. It has the form of a turbulent Reynolds number,  $\delta_0/\delta_v = u_\tau \delta_0 / v \equiv Re_\tau$ , and since the Reynolds number is large in turbulent flow, the outer

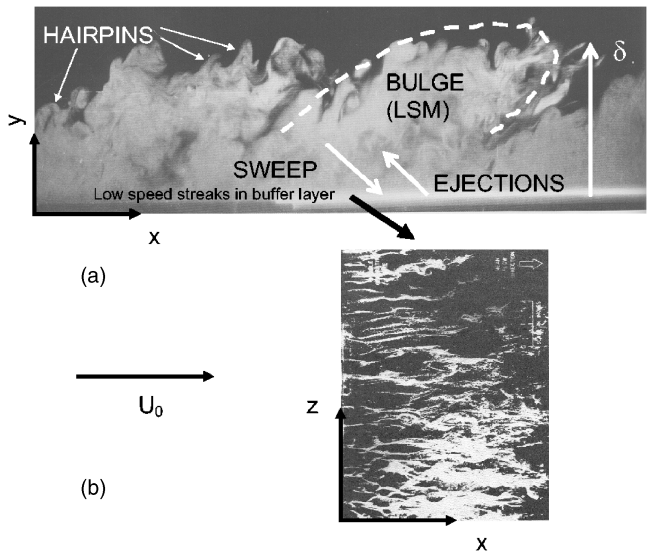


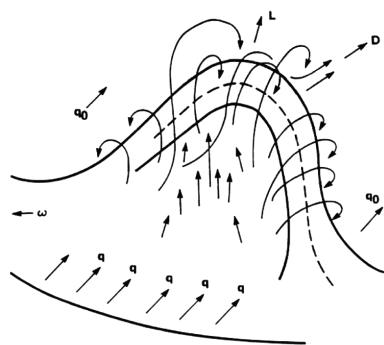
FIG. 2. (a) Smoke visualization of the streamwise-wall-normal plane in a turbulent boundary layer showing various eddy structures (from Ref. 5); (b)  $H_2$  bubble visualization of low-speed streaks in a streamwise-spanwise plane (from Ref. 11).

length scale is necessarily large compared to the viscous length scale. Thus, wall flows are inherently inhomogeneous. von Karman's logarithmic law can be derived by postulating a length scale  $\ell = \kappa y$ , where  $\kappa$  is von Karman's constant, and writing  $dU/dy = u_\tau/\kappa y$ . This suggests a physical picture in which the size of the eddies is a constant proportional to  $\delta_v$  close to the wall, increases nearly linearly across the logarithmic layer, and approaches a constant proportional to  $\delta_0$  in the part of the outer region (usually referred to as the wake). Perhaps the second most interesting question surrounding wall turbulence is exactly how the eddies change so as to accomplish this variation of length scale. The scaling with  $y$  also suggests that the structure in the logarithmic layer is self-similar, raising a question as to the form of the self-similar eddies.

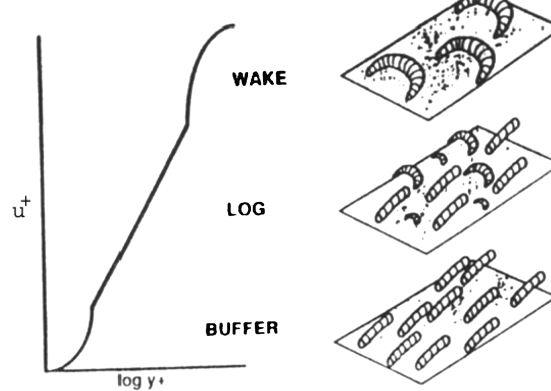
A well-known visualization of a low Reynolds number turbulent boundary layer by Falco,<sup>5</sup> Fig. 2(a), illustrates several of the known types of coherent structures. The patterns that are most visible reside near the boundaries between clear regions and smoke-filled regions, mainly near the outer edge. There, one can see the large-scale motions (LSMs) or *turbulent bulges*<sup>5–8</sup> having length of order 2–3  $\delta$ . LSM occurs in all of the canonical wall flows. Sweeps and ejections cannot be seen in this type of visualization, but their presence is indicated for reference.

Atop the bulges, there are many structures inclined about 45 degrees to the wall. Several take the form of hairpin-shaped loops resembling the *horseshoe vortex* proposed by Theodorsen.<sup>9,10</sup> In his conceptual model of the horseshoe vortex, Fig. 3(a), Theodorsen visualized a vortex filament oriented spanwise to the mean flow, and perturbed by a small upward motion. The part of the filament lying further away from the wall (variously called the *head* or the *arch*) would experience higher mean flow velocity and be convected downstream faster than its lower-lying parts. Consequently, the legs connecting the spanwise part of the vortex to the

(a)



(c)



(b)

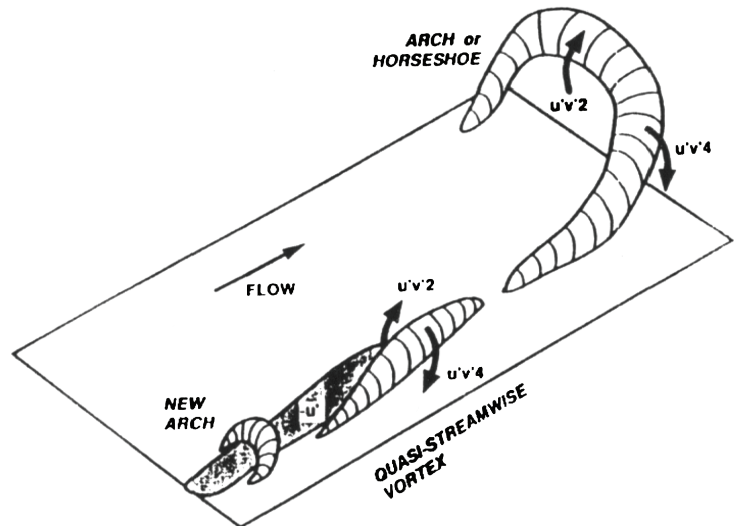


FIG. 3. (Color) (a) Theodorsen's (1952) depiction of a horseshoe vortex (from Ref. 9); (b) sketch of "The Horseshoe" attributed to Weske (courtesy of J. Wallace, University of Maryland); (c) Robinson's summary of structures found in direct numerical simulation of wall turbulence (from Ref. 12).

head would be stretched and intensified, causing the vortex to lift away from the wall into still higher mean velocity, resulting in still greater stretching. Being purely kinematic, this instability is easy to understand.

Theodorsen<sup>10</sup> supported his ideas with smoke visualizations attributed to Weske, and Weske is also believed to have made the beautiful sketch of a horseshoe presented in Fig. 3(b) (provided by courtesy of J. Wallace, University of Maryland). Interestingly, the drawing also indicates smaller-scale hairpin vortices on the larger horseshoe, i.e., a hierarchy of scales, although it is not clear that such patterns were actually observed. In fact, the technology of the day did not permit measurement of vorticity, which would have established that the loops of smoke were, indeed, vortices. Moreover, in all but low Reynolds number flows, it was extremely difficult to visualize structures in the interior of the flow, where Theodorsen imagined them to occur first.

Figure 2(b) shows the long streamwise streaks of H<sub>2</sub> bubbles reported by Kline, *et al.*<sup>11</sup> in a plane close to the wall. These streaks were shown to be regions of low streamwise momentum, and in the buffer layer their mean spanwise

spacing was found to be approximately 100 viscous wall units, one of the more reliable physical constants in the study of turbulence. Later, the low-speed regions were associated with quasistreamwise vortices lifting viscously retarded fluid upwards from the region close to the wall (cf. Robinson<sup>12</sup> for a summary of the evidence). Observations of bubbles in x-y planes also revealed the sequence of events that came to be known as *bursting*, in which the bubble streaks wavered vertically with increasing amplitude and then lifted away from the wall in a vigorous, chaotic motion. The bursting concept excited considerable interest, and many subsequent researchers sought mechanisms to explain the origin of explosive upward motions, using quadrant analysis of time series data to identify events occurring before and after the signatures of bursts. Of particular note is the mean tendency of Q2 events to be followed almost immediately by somewhat longer duration Q4 events, and the fact that Q2 events tend to occur in groups. It was not until almost two decades after the first observation of bursts that Bogard and Tiederman<sup>13</sup> and later Tardu<sup>14</sup> were able to show that bursts are actually a sequence

of increasingly stronger ejections, rather than individual ejections.

While the bursting model was received well, Theodorsen's horseshoe model met less enthusiasm. The reasons are not clear, but perhaps some of the early resistance stemmed from Theodorsen's ideas preceding the concept of coherent structures. In contrast, the bursting concept was developed at a time when coherent structures were gaining credibility. Also, the approximately two-dimensional low-speed streaks were easier to observe than three-dimensional vortices, and they occurred in the buffer layer, where the mean velocity changed the most in low-to-moderate Reynolds number flows. Thus, the reasoning went that even if hairpin vortices did occur, they were not likely to be as important as the low-speed streaks and their attendant quasistreamwise vortices.

Much later, experimental studies of horseshoe vortices (also known as horseshoe eddies, hairpin vortices, and hairpin eddies) by Head and Bandyopadhyay<sup>15</sup> and Bandyopadhyay<sup>16</sup> pioneered renewed interest in them as fundamental elements of the turbulent wall layer. Their visualizations used smoke and inclined light sheets to show that inclined structures consistent with hairpins existed in abundance over a range of Reynolds numbers downstream of transition. They proposed a model in which hairpins having spanwise width of approximately  $100\delta_v$ , extended from the wall up to the top of the boundary layer in a succession of increasingly taller hairpins. This inference appears to have been based mainly on the observation that the spacing between the legs of the hairpins near the edge of the smoke-filled region, where the loops could be observed as in Fig. 2(a), was 100 viscous wall units even at elevated Reynolds numbers. This was a puzzling result because, if extrapolated to very high Reynolds number, it implied that very thin eddies could maintain their size from the ground to the top of the atmospheric boundary layer, for example. It seems more likely that the size of the hairpins increases with distance from the wall, and the thin eddies observed at the edge of the boundary layer were actually created locally, rather than being attached to the wall.

Smith<sup>17</sup> also succeeded in visualizing hairpins in low Reynolds number water flows using videos of H<sub>2</sub> bubble patterns, and he observed the formation of successive in-line hairpins. This stimulated a series of investigations of hairpins generated artificially by wall-mounted hemispheres and low-momentum wall jets that culminated in an important article discussing theoretical mechanisms by which successive hairpins could be formed.<sup>18</sup> Perry and Chong<sup>19</sup> and co-workers<sup>20,21</sup> made the most serious theoretical use of Theodorsen's horseshoe vortex paradigm by constructing a model of individual hairpins scattered randomly in the streamwise-spanwise plane and containing a hierarchy of sizes. In their model, the location of each hairpin was statistically independent of every other hairpin. With appropriately chosen parameters for the hairpin geometry and the distribution of the hierarchy, the model reproduced many aspects of statistical quantities such as mean velocity, Reynolds stresses, and spectra, but it encountered difficulty with the low-wave-number end of the spectrum.<sup>21</sup>

The large-eddy simulations of turbulent channel flow by Moin and Kim<sup>22–24</sup> provided the first three-dimensional evidence for hairpin vortices that was based on vorticity. Visualizations of instantaneous vortex lines looked like omega-shaped hairpins, and conditional averages given ejection and sweep events looked like extended perturbations of vortex sheets. Robinson,<sup>12</sup> working with Kline,<sup>25</sup> performed a very careful study of structures found in direct numerical simulation of the low Reynolds number boundary layer.<sup>26</sup> Figure 3(c) reproduces Robinson's summary of the structures he commonly observed: quasistreamwise vortices close to the wall, arches or horseshoe vortices in the wake region, and a mixture of quasistreamwise vortices and arches in the logarithmic layer. He used the term "arches" to distinguish between fully formed omega-shaped vortices resembling somewhat broadened hairpins and the top of a horseshoe minus its legs, i.e., not extending down to the wall. The infrequent observation of complete hairpins or horseshoes appears to have stopped Robinson short of fully embracing the hairpin vortex model, but it may have been attributable to the visualization method that was employed. Robinson also observed two horseshoe-like structures in succession, similar to the experiments of Smith.<sup>17</sup>

Visualizations of structure in LES and DNS<sup>22–25</sup> were watersheds in the study of wall turbulence because they were based on three-dimensional data that made full fields of velocity, vorticity, and pressure available for visualization. Even with full data, the visualization of vortices was difficult, and it remained an unsettled subject in its own right (cf. Refs. 27 and 28 and references therein). But, at least it could be proven that arches looking like loops of smoke were indeed vortices, and that low-speed streaks were associated with quasistreamwise vortices, as had been proposed earlier.<sup>29</sup> Since then, direct numerical simulations at ever increasing Reynolds number have provided a fundamental new tool for studying turbulence structure. The year 1991 also saw significant developments in the theory and the experimental structure of wall turbulence. Smith, Walker, Haidari, and Sobrún<sup>18</sup> published a theoretical analysis of a mechanism to explain the creation of successive hairpins, and visualizations of spanwise vorticity fields in channel flow based on particle image velocimetry (PIV) were published showing vorticity patterns consistent with near-wall hairpins.<sup>30</sup> In succeeding years, PIV critically complimented DNS by allowing two-dimensional measurements at higher Reynolds number in flows that were unequivocally "real." These new tools, DNS and PIV, provided the means to remove many of the uncertainties that undermined the acceptance of earlier conceptual models discussed above and to refine and unify them. The purpose of this paper will be to summarize the developments that have occurred since 1991. We will see that with a few relatively minor modifications and a few critical new ideas, a relatively simple, cohesive picture has emerged that is both consistent with earlier work and stimulative of future work.

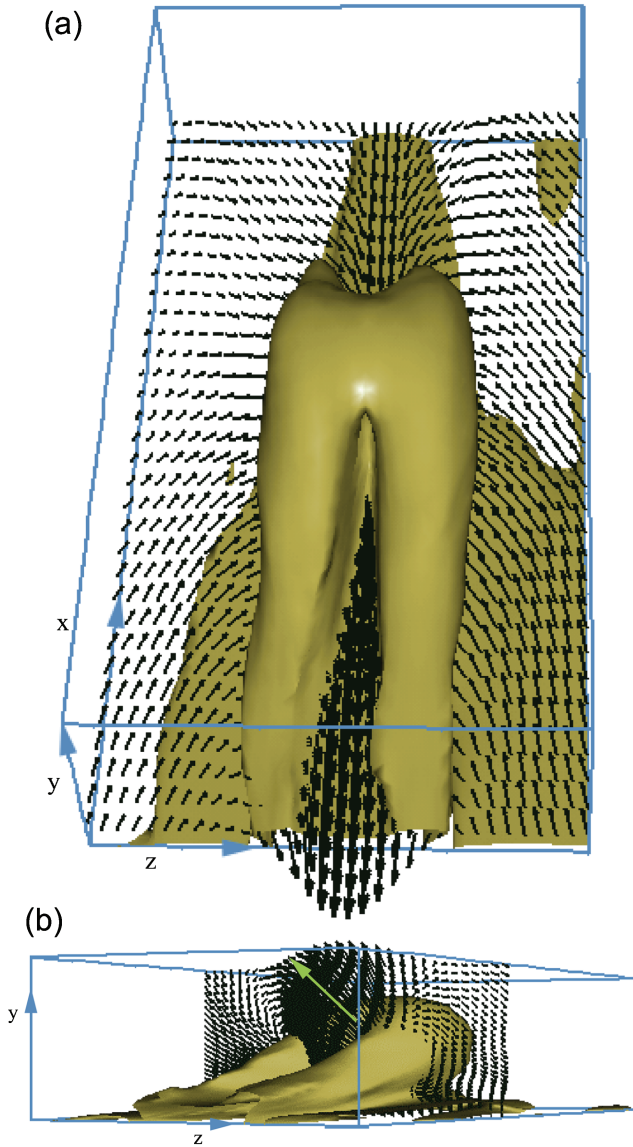


FIG. 4. (Color) Conditional average of the flow around a Q2 event velocity vector ( $(u, v, 0)$  located at  $y^+=49$ ) in a direct numerical simulation of channel flow at  $Re_\tau=300$ . The surface is an iso-contour of the turbulent swirling strength,  $\lambda_{ci}$ , and the vectors denote fluctuations. (a) top view; (b) oblique view (from Ref. 31).

## II. NEAR-WALL HAIRPIN EDDY PARADIGM

The question concerning the form of the eddies that create Reynolds shear stress can be addressed without bias by determining the mean turbulent flow field about a point where the flow makes a strong contribution to the mean Reynolds shear stress. The mean is given by the conditional average of the fluctuating velocity given a velocity at the fixed point  $\mathbf{x}_0$ ,  $\langle \mathbf{u}(\mathbf{x}, t) | \mathbf{u}(\mathbf{x}_0, t) = \mathbf{u}_0 \rangle$ . There are two values of the velocity vector that maximize the integrand in the integral for  $\overline{-uv} = -\int uv f(u, v) du dv$  ( $f$  is the joint probability density function). The value at the maximum that is located in the second quadrant, i.e., an ejection event, is of special interest because these events prevail outside the buffer layer. The conditional eddy given an ejection at  $\mathbf{x}_0$  in a DNS of channel flow<sup>31</sup> is visualized in Fig. 4 by plotting isosurfaces of the

turbulent swirling strength,  $\lambda_{ci}$ , defined as the imaginary part of the complex eigenvalue of  $(\nabla(\mathbf{u}|\mathbf{u}_0))\mathbf{x} = \lambda\mathbf{x}$ . Swirling strength is one of several kinematic quantities that yield qualitatively similar visualizations of a vortex. It is like vorticity, except that it corresponds to the part of vorticity associated with rotation, and it discriminates against the contribution made by shear (cf. Ref. 28). The conditional eddy given an ejection event clearly takes the form of a hairpin eddy. In Fig. 4, it is symmetric about the  $x$ - $y$  plane because the event vector was given a zero spanwise component. An event with nonzero spanwise velocity yields a cane-shaped eddy, i.e., one leg stronger than the other, and asymmetry is known to be the most probable condition.<sup>32</sup>

The conditional eddy is a combination of a hairpin eddy and two relatively short counter-rotating quasistreamwise vortices. Flow is swept up from around the eddy and thrust upwards in a strong ejection inboard of the head of the eddy and the legs. Vortex induction from the vorticity elements in each leg and in the head is focused in this region, so as to create a concentrated flow. In the outboard regions of the vortex, fluid flows down and forward, forming a sweep. It is weaker than the ejection because the induction from the vortex elements is unfocused. Near the wall (less than  $y^+ \approx 15$ ) the induction of the quasistreamwise vortex legs lifts viscously retarded fluid upwards causing low speed streaks, as usual, but the vectors are inclined at much shallower angle than the conditional ejection event. Note that the isosurface has two weak protrusions on the downstream face of the head. These appear to be real manifestations of the structures that go into the conditional average, and they will be discussed later.

The conditionally averaged structure suggests a modernization of Theodorsen's horseshoe that combines the horseshoe head with quasistreamwise vortices into a single eddy,<sup>33</sup> as indicated schematically in Fig. 5. The sketch recognizes that eddies are seldom if ever perfectly symmetric, and they are usually distorted by other eddies in the turbulent environment. Because of vortex induction, the eddy propagates in the direction of the Q2 vectors relative to the surrounding flow, much like a vortex ring. In a frame moving with the eddy, the surrounding flow appears to be a Q4 event, and hence a stagnation point forms where the Q2 and Q4 flows cancel. This effect probably accounts for the famous VITA transition from Q2 to Q4 events observed in time series from hot-wire studies.<sup>34</sup> The opposing Q2/Q4 flows create the inclined shear layer reported in a number of studies (cf. Ref. 12).

Figure 5(b) depicts the characteristic flow elements that would be seen in an  $x$ - $y$  plane cutting through the hairpin eddy of Fig. 5(a): the compact region of vorticity in the head, the Q2 flow with an orientation approximately perpendicular to the plane containing the head and neck of the hairpin, the Q4/Q2 stagnation point, and the low-speed streak next to the wall. This combination of flow elements is called the *hairpin vortex signature*.<sup>33</sup> It is found with high frequency in PIV studies of pipe, channel, and boundary layer flow at Reynolds number ranging from low to moderate.<sup>33,35</sup> Perry and Chong<sup>19</sup> show that a simple vortex model shaped like a goal post or a lambda produces a very similar pattern.

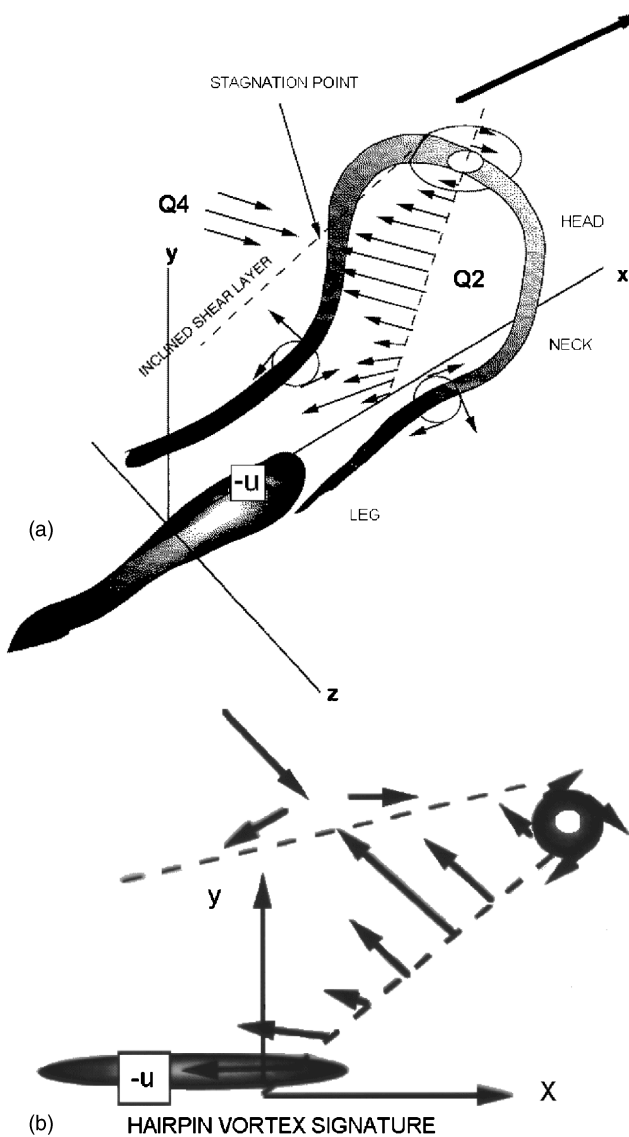


FIG. 5. (a) Schematic of a hairpin eddy attached to the wall; (b) signature of the hairpin eddy in the streamwise-wall-normal plane (from Ref. 33).

An example of several hairpin vortex patterns from an experimental boundary layer is presented in Fig. 6. The heads of the hairpins are labeled A–D and the reader can see by inspection where the other elements of the hairpin vortex signature occur. Note that the Q2 vectors fall along regions inclined at about 45 degrees to the wall, as in Ref. 15, and each Q2 event has a local maximum of the flow speed. The consistent formation of maxima is key evidence for inferring the existence of a hairpin head and neck from the planar PIV data. A straight spanwise vortex would not produce the observed maximum, and the induced flow would be more axisymmetric. The important effect of the curvature of the head and necks of the hairpin is to focus induction in the inboard region and defocus it in the outboard region, consistent with the Q2 events being stronger (greater speed) than the Q4 events above the legs.<sup>33</sup>

To summarize, the single hairpin eddy is a useful paradigm that explains many observations in wall turbulence. In particular, it provides a mechanism for creating Reynolds

shear stress, low-speed streaks, and for transporting vorticity of the mean shear at the wall away from the wall and for transforming it into more isotropically distributed small-scale turbulent vorticity.

### III. HAIRPIN VORTEX PACKETS

The discussion thus far has concentrated on the single hairpin or horseshoe vortex, but as noted in the Introduction there is evidence in earlier studies that hairpins occur in streamwise succession, with size increasing downstream.<sup>15–18,33,35–37</sup> The pattern of hairpin vortex signatures A–C in Fig. 6 is consistent with these observations, and patterns like this are observed with high frequency in PIV data.<sup>33</sup> A major conclusion of the PIV study was that hairpins occur most often in *packets*, so named because the individual hairpins travel with nearly equal velocities, i.e., the groups of hairpins form packets having relatively small dispersion in their velocity of propagation. Recall that long life is one of the major prerequisites for a coherent structure, and to be long-lived, dispersion must be small. Adrian *et al.*<sup>33</sup> report dispersion less than 7% at the Reynolds numbers they studied.

The mechanisms that lead to the formation of hairpins in packets have been explored by analysis<sup>18</sup> and by numerical studies of packet growth.<sup>36,37</sup> An example of a packet pattern computed using DNS of fully turbulent channel flow is presented in Fig. 7(a). The packet evolves from an initial velocity field consisting of a three-dimensional conditional eddy similar to that in Fig. 4 plus a turbulent mean flow profile. The initial conditional eddy rapidly changes into an omega-shaped hairpin with trailing legs looking much like the sketch in Fig. 5. The distance between its legs is about  $100\delta_v$ , and the height of its head, once formed into a mature omega, is also about  $100\delta_v$ . After attaining a mature omega shape, the primary hairpin continues to grow in all directions, and two new hairpin heads are formed: a downstream hairpin vortex (DHV) and a secondary hairpin vortex (SHV). The SHV is created by the interaction of low-speed fluid being pumped upwards by induction between the legs with high-speed fluid above the legs, leading to a vortex roll-up that forms an arch. The necks develop under the arch of the SHV and merge with the legs. In the flow that produces Fig. 7(a), the SHV generates another upflow, leading to the formation of a tertiary hairpin vortex, and so on. The DHV is formed when the protrusions on the downstream face of the conditional eddy are pulled out into a pair of nearly streamwise vortices that then act like the wall-attached legs to induce an upward flow that rolls up into the arch of the DHV. Note, however, that the DHV appears to be detached from the wall. New quasistreamwise vortices are also generated very close to the wall and beside the legs of the hairpins. They have been attributed to the Brooke-Hanratty mechanism<sup>38</sup> in which the outboard downwash induced by a leg separates at the wall and rolls up to form a new vortex rotating counter to the original.

The formation of new hairpins is called *auto-generation*.<sup>36,37</sup> It is a nonlinear process, in the sense that it only occurs if the magnitude of the event vector used to

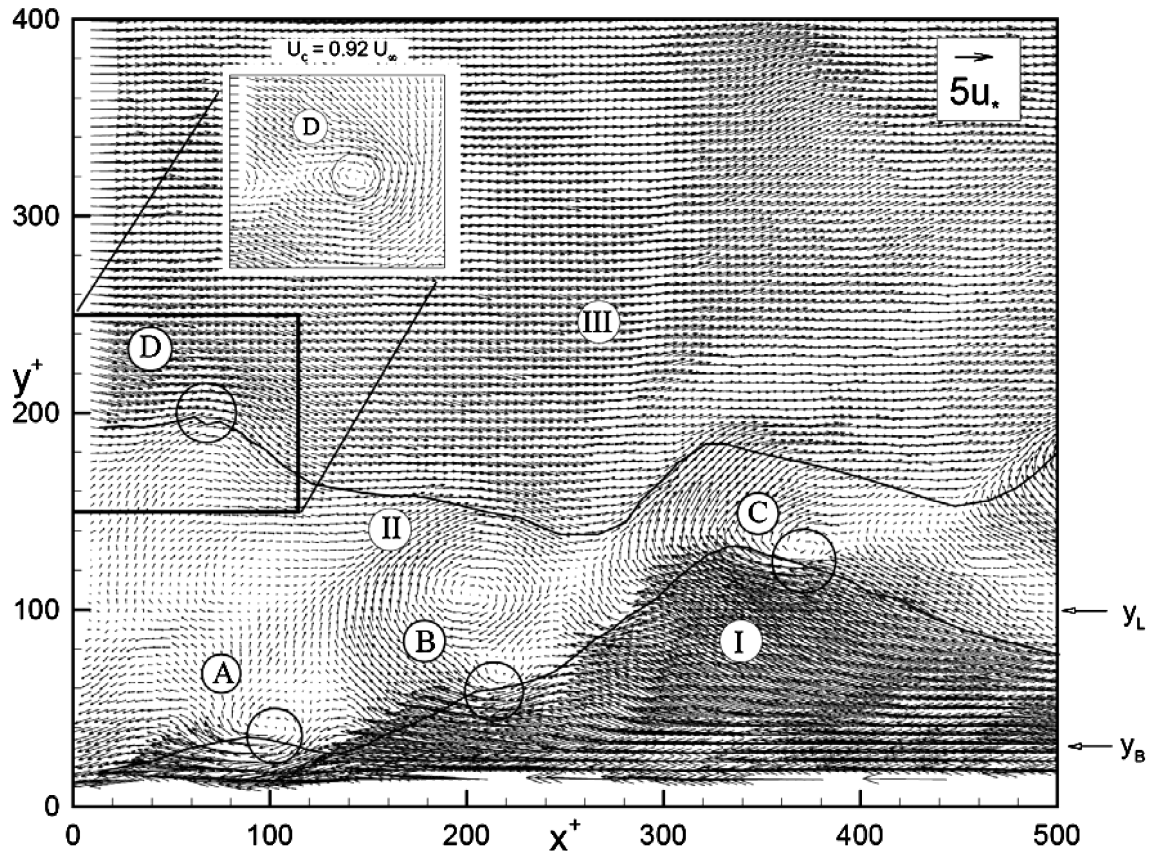


FIG. 6. Hairpin vortex signatures in a PIV measurement of flow in the streamwise-wall-normal plane of a turbulent boundary layer,  $\text{Re}_\theta=930$ . The heads of the hairpins are labeled A, B, C, and D. Note the correspondence between the flow patterns below and behind each head with the hairpin signature sketched in Fig. 5(b). Zones of uniform momentum are labeled I, II, and III. The reference frame for the vectors is translating at 80% of the free-stream velocity (from Ref. 33).

define the initial conditional eddy exceeds a threshold value. Below the threshold, the eddy evolves into an omega-shaped hairpin that gradually dissipates. Above the threshold, new hairpins autogenerate for as long as the computations can be performed before the packets run out of space in the computational domain. The threshold value depends weakly on several factors, but typically it is about  $(u, v) = (1.5\sigma_u, 1.5\sigma_v)$ . Values this large or larger occur in no more than 5–10% of all Q2 events, but this fraction is consistent with the relatively small number of Q2 events needed to fill the volume with hairpin packets (cf. Fig. 9).

Figure 7(b) is the last frame ( $t^+=355$ ) of a movie showing the growth of a packet out of a symmetric conditional Q2 eddy. The video can be viewed in the file that is attached to Fig. 7 online. It shows the development described above, with two modifications. First, in the very early development, the stretching of the downstream protrusions creates a series of hairpin arches above them with spacing equal to twice the streamwise grid spacing. These are numerical artifacts associated with the initial rapid transient growth, but by  $t^+=100$  they have dissipated and after this time computations with various grid resolutions all yield nearly the same result. Second, the tertiary hairpin in the movie simulation develops at a location between the primary and the secondary hairpin, instead of the location upstream of the secondary hairpin found in the lower Reynolds number computation of Ref. 37.

This vortex may be the start of a new hairpin vortex packet forming inside the environment created by older, larger hairpins, as described in the hierarchical scenario to be discussed later. Despite minor differences, the overall forms of the simulated packets in Figs. 7(a) and 7(b) are quite similar.

As the upstream hairpins grow, they lift the quasistreamwise vortices upwards, and ultimately these vortices appear to come out of the downstream sides of the hairpin. They are the likely sources of the protrusions in the initial conditional eddy.

The packets in Fig. 7 resemble the groups of eddies computed in transitional turbulence<sup>39</sup> in many aspects. The principal distinction between the transitional computation and the present turbulent computations lies in the Blasius base flow for transitional study versus the turbulent mean flow for the turbulent study. The latter has much higher shear rate at the wall and an inner scale independent of the outer scale.

The packets in Fig. 7 and in the movie each start from a Q2 event that has zero spanwise velocity. Hence, they evolve into packets that are reflectionally symmetric about the  $x$ - $y$  plane containing the Q2 event vector. If the spanwise velocity of the Q2 event is nonzero, as is more probable, then the packets break this symmetry and the successive hairpins are shaped like canes.<sup>37</sup>

Interestingly, a small amount of noise added to the initial

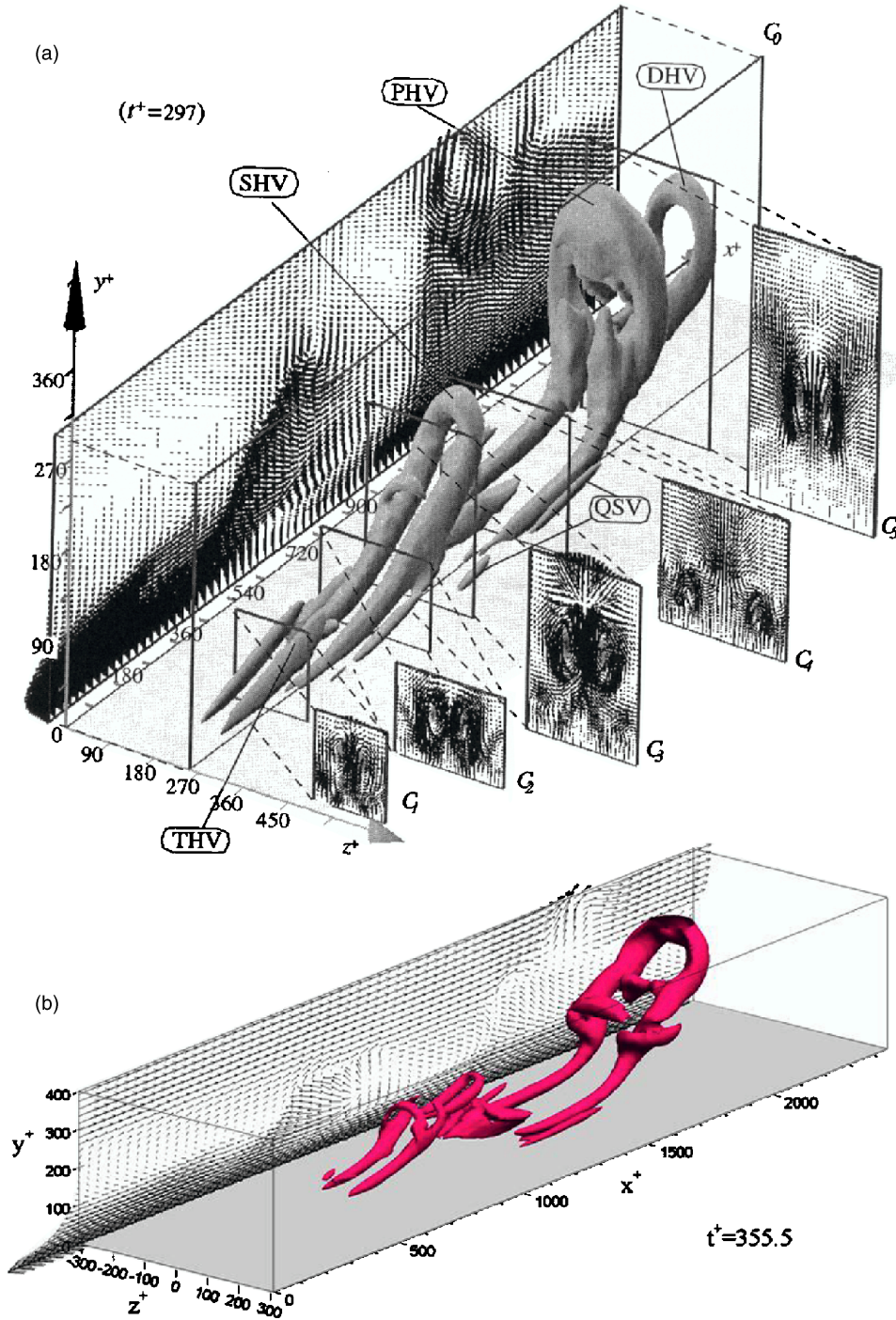


FIG. 7. (Color online) (a) Packet of hairpins that evolves from a conditional Q2 event ( $w=0$ ) similar to that shown in Fig. 4. The shaded surfaces are isosurfaces of the swirling strength. The time is 297 viscous time scales after the initial condition, and the channel flow Reynolds number is  $Re_\tau=180$  (from Ref. 37). (b) Last frame of the digital movie. Evolution of a packet of hairpins from a conditional Q2 event similar to that shown in Fig. 4. Surface is an isosurface of the swirling strength. The Reynolds number is  $Re_\tau=395$  (courtesy of K. Kim) (enhanced online).

condition leads to chaotic development of the hairpin packet.<sup>31</sup> The packet in Fig. 8 evolved from a Q2 conditional hairpin plus approximately 5% noise. The movie in the file attached to Fig. 8 online shows this evolution. Following a brief period in which the gradients of the noise are large, but rapidly dissipating, the first hairpin forms, and the autogeneration process follows a sequence similar to that for the symmetric hairpin, except that the tertiary hairpin forms at the location of the secondary hairpin, at least for the handful of noise fields that have been computed.

The most interesting property of the chaotic packet is that it retains the same general properties as the clean packet, despite the sensitivity of the field in detail. Autogeneration

occurs, the distance between successive vortices is about the same, and the vertical and spanwise growth rates of the hairpins are about the same, as shown by the growth angles of the clean and chaotic packets being similar. These similarities clearly imply that the autogeneration mechanism is robust, and robustness is consistent with turbulence being random, yet having reproducible statistical properties. The hairpins that are formed upstream of the primary vortex meet Townsend's<sup>1</sup> definition of an *attached eddy*, having a size proportional to the distance from the wall.

The simulations of individual packets do not prove that such packets occur in real turbulent flows, and the two-dimensional PIV evidence in fully turbulent flow relies on

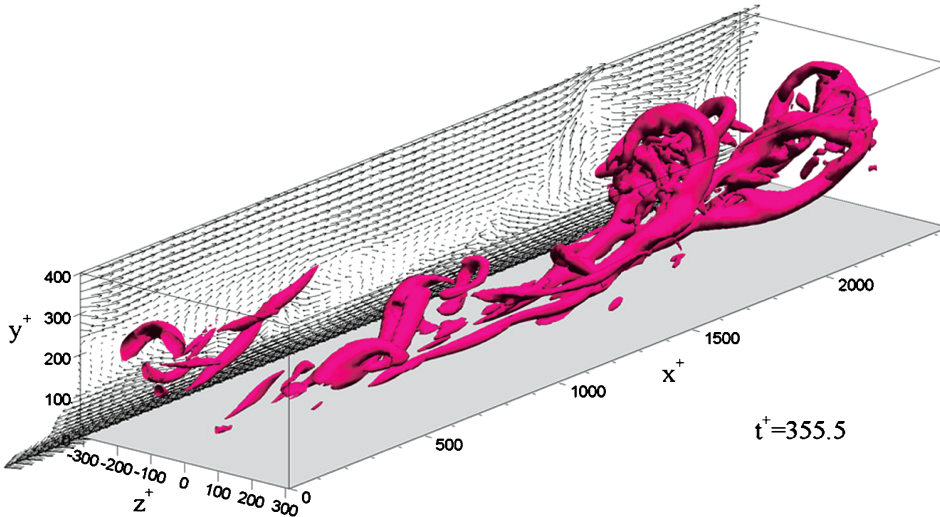


FIG. 8. (Color) Chaotic packet of hairpins that evolves from an initial conditional Q2 event ( $w=0$ ) similar to that shown in Fig. 4 with 5% noise added to simulate growth in a slightly turbulent environment. The time is 355 viscous time scales after the initial condition and the channel flow Reynolds number is  $Re_\tau=395$  (courtesy of K. Kim) (enhanced online).

inferring three-dimensional structure from two-dimensional data. It would seem like the most direct method of observing hairpin packets would lie in the careful visualization of DNS of fully turbulent wall flows. Unfortunately, visualizing hairpins in fully turbulent DNS flows proved to be difficult for many years, partly due to the complexity of fully turbulent flow and partly due to the issue of identifying vortices. Even the visualization of a single three-dimensional hairpin shape in turbulent channel flow simulated by DNS awaited the work of Chacin, Cantwell, and Kline<sup>40</sup> (almost a decade after the channel flow simulation of Kim, Moin, and Moser<sup>41</sup>). This careful study provided some of the best evidence for the existence of hairpins, albeit at low Reynolds number.

Evidence from a relatively recent study<sup>31</sup> showing the existence of three-dimensional packets in DNS of fully turbulent channel flow is reproduced in Fig. 9. By visual inspection, all of the vortices resembling hairpins were highlighted in white, without bias toward any particular arrangement. Once the individual hairpins were identified, the arrangement in the form of a hairpin packet (or perhaps two hairpin packets each containing four to five hairpins) was clear. The spanwise growth angle, about  $12^\circ$ , and a similar vertical growth angle (not shown) agreed well with the PIV data and with the single-packet simulations. Interestingly, the chaotic structure in the fully turbulent flow is qualitatively similar to the structure of the chaotic hairpin packet in Fig. 8, in the same broad sense that the chaotic packet resembles the clean packets, as discussed above. The fully turbulent packet pattern is not significantly more complex than the packet in Fig. 8, although it appears to be immersed in considerable small-scale vortex debris. (The concept of organized structure in a sea of random vortices can already be found in Ref. 19.) The similarity further supports the idea that packets grow and evolve in a robust manner whether they are stimulated by an initial disturbance in a clean environment or occur naturally in a fully turbulent environment.

In the results presented thus far, the Reynolds numbers are relatively low, leaving open questions concerning the existence and form of packets at high Reynolds number. First,

higher Reynolds number LES and DNS results<sup>42,43</sup> contain such large numbers of small-scale vortices that three-dimensional packets are not easily recognized by eye or by systematic three-dimensional image analysis. Second, at Reynolds numbers that are accessible to DNS with current computers, the hairpins have viscous cores with circulation Reynolds numbers of order 10–30. Can such flow entities persist at very large Reynolds number or will they become unstable? Third, by the time packets grow to fill the low Reynolds number channel flows in Figs. 7–9, they only contain three to four hairpins. Increasing the Reynolds number



FIG. 9. Hairpin packets can be observed in DNS of fully turbulent channel flows.  $Re_\tau=300$ . The heads of hairpins that appear to be members of one or perhaps two packets are indicated in white. Note the large amount of disorganized small-scale clutter (from Ref. 31).

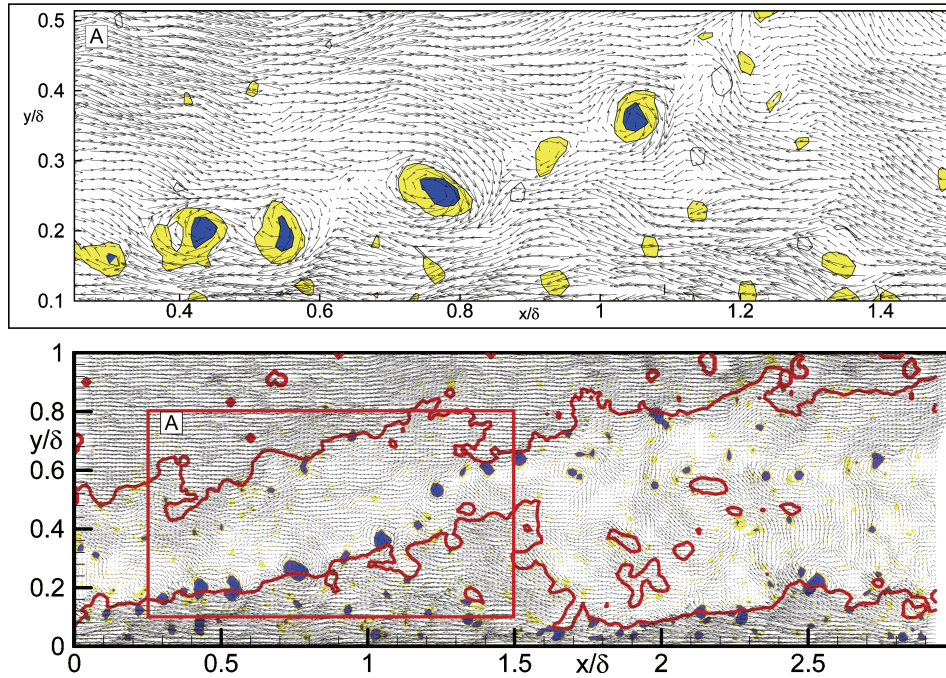


FIG. 10. (Color) Hairpin packets are observed very commonly in high Reynolds number laboratory flows. The PIV data in this figure show that long packets occur inside even larger packets. The color contours are swirling strength in the lower plot and spanwise vorticity in the upper, expanded plot. The vectors are total velocity minus 76% of the free stream velocity (lower plot) and 79% of the free-stream velocity (upper plot) (from Ref. 33).

effectively makes more room for the packets to grow<sup>33,44</sup> so that packets would contain more hairpins and may become more complex at higher Reynolds number. (Recall that hairpins reach a mature shape when they are nominally 100 viscous wall units tall, making the ratio of the tallest hairpin to the smallest hairpin  $\delta_0/100\delta_v \approx Re_t/100$ .) Would such large packets be sustainable? Lastly, would the increasing multi-

plicity of scales or some new mechanisms that develop at large Reynolds number disrupt the autogeneration mechanism or supplant the packets?

Partial answers can be found in the higher Reynolds number data in Figs. 10 and 11. The Reynolds number of the boundary layer in Fig. 10 ( $Re_\theta=7705$ ,  $\delta^+ \approx 2250$ ) is about eight times larger than that in Fig. 6. Several long, ramp-

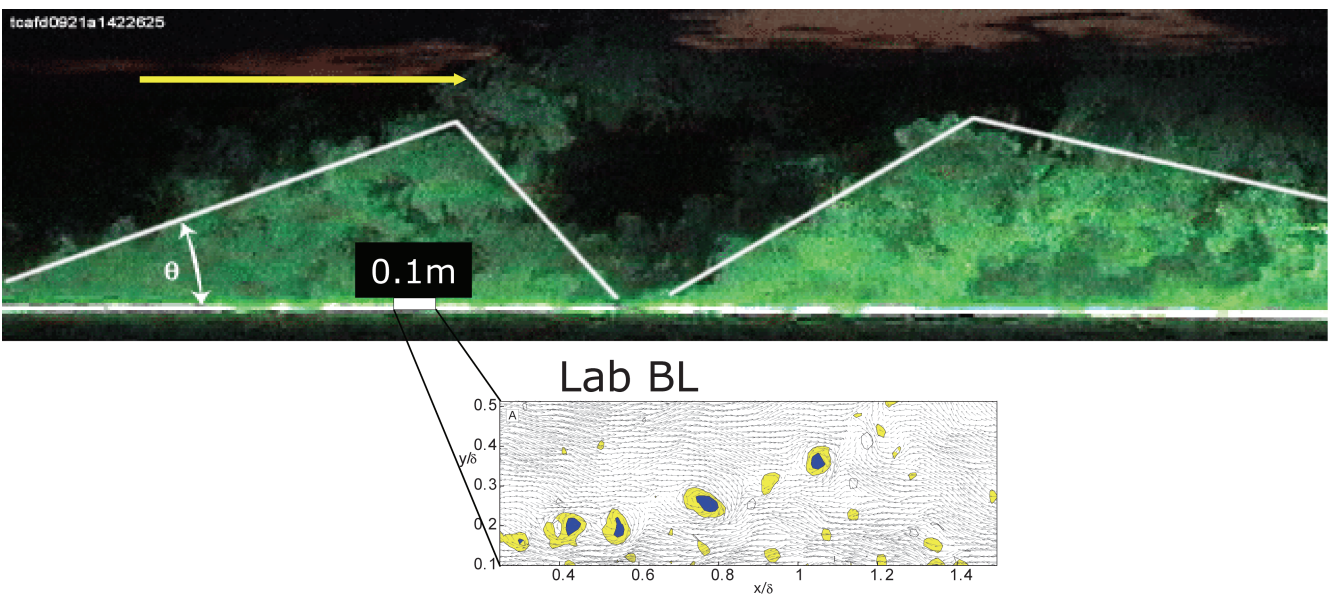


FIG. 11. (Color) (a) Ramp-shaped patterns consistent with hairpin packets such as those in Fig. 10 can also be found in the atmospheric boundary layer. Smoke emitted from the floor of Utah's Great Salt Lake desert is illuminated in the streamwise-wall-normal plane by a Nd: YAG laser light sheet. The scale is 2 m from the floor to the top of the figure. The PIV visualization of the laboratory boundary layer from Fig. 10 is shown for comparison (from Ref. 45). (b) Video sequence of the ramps observed in the atmospheric boundary layer described in (a) (enhanced online).

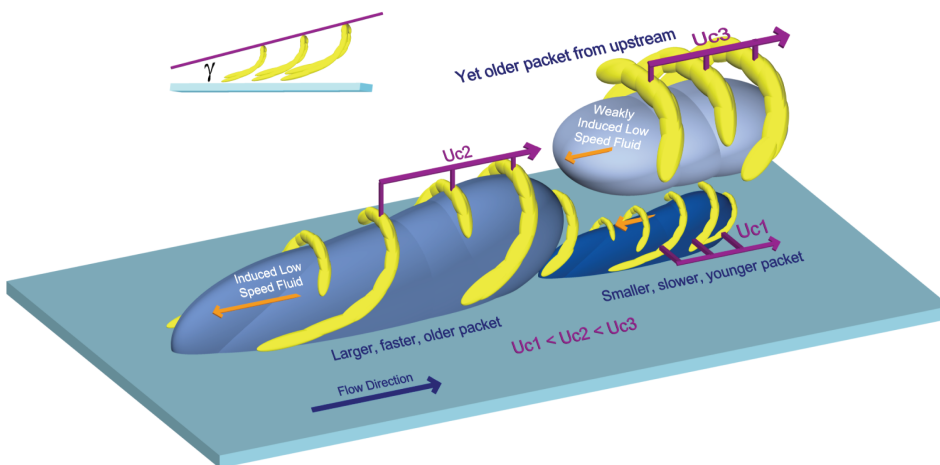


FIG. 12. (Color) Conceptual scenario of hairpins attached to the wall and growing in an environment of overlying larger hairpin packets (from Ref. 33).

shaped packets extend beyond the logarithmic layer (nominally at  $0.1\text{--}0.2 \delta$ ) and across almost the entire boundary layer. They are reminiscent of the drawing in Bandyopadhyay.<sup>16</sup> As expected, there are more vortex heads per packet than in lower Reynolds number flow. To reach more convincing Reynolds numbers, the visualization in Fig. 11 was performed in a neutrally stratified, nearly steady atmospheric boundary layer over a nearly smooth desert floor by injecting smoke through a slot in the floor and illuminating it with a laser light sheet.<sup>45</sup> Videos of the region from the floor to 2 m elevation revealed ramp-shaped patterns like Fig. 11 and patterns consistent with vortex heads on the boundaries between the clean and the smoke-filled regions in virtually every frame. (See the movie in the file attached to Fig. 11 online.) The boundary layer depth of this flow was estimated at 200 m, so the smoke visualization occurred well within the logarithmic layer, in this case. For comparison, a small rectangle in Fig. 11 indicates the physical extent of the laboratory flow in Fig. 10. Quantitative PIV measurements of ramps structures have also been made in the atmospheric boundary layer more recently.<sup>46</sup> Thus, among Figs. 6, 10, and 11 we see packets in a low Reynolds number flow with almost no logarithmic layer, in a region outside of the logarithmic layer of a moderate Reynolds number flow, and in a region very deep within the logarithmic layer in a virtually infinite Reynolds number flow.

The ramps in Fig. 10 are evident visually because the streamwise velocity inside each ramp is quite different from the velocity outside the ramp and relatively constant inside it. Visualizations of these *zones of uniform momentum* in PIV data and histogram analysis of the velocity have shown that multiple uniform momentum zones exist through the boundary layer and are prevalent as ramp-shaped structures for laboratory Reynolds numbers.<sup>47</sup> They have been attributed to the effect of *coherent vortex induction* inside hairpin vortex packets.<sup>33</sup> This phenomenon results from the addition of the induced fields of the hairpins, and it is analogous to the addition of the magnetic fields induced by the multiple windings of a solenoid. The effect of adding the backward induced flows together is illustrated clearly in Fig. 6, wherein the dark region under vortex heads A-C corresponds to strong negative streamwise velocity fluctuation, and simi-

larly for the dark regions under the ramps in Fig. 10. The larger the packet, the weaker the backward induced flow, owing to the greater mean distance from the vortex elements in the hairpin cores to the center of the hairpin loop.

The coincidence between the loci of the heads of the vortices and the change in velocity from one momentum zone to another combined with the model for coherent vortex induction are the principal reasons for concluding that the low-momentum zones are the interiors of hairpin packets. Contour plots of streamwise momentum show clearly that zones, i.e., packets, occur within the flow fields of larger packets.<sup>33</sup> The change in velocity between zones occurs because the larger packets induce weaker backward flow. Thus, at any instant the turbulent flow is a summation of contributions from a hierarchy of different sized packets. And, as noted above, within each packet, the flow field is also a sum of contributions from the induced fields of a collection of hairpins, so there are really three (not necessarily independent) scales: those arising from the hairpins and their cores, the packets, and the hierarchy of packets.

The situation is sketched schematically in Fig. 12. The coherent alignment of vortices creates an induced backflow region inside the packet that is much longer than the backflow induced by a single vortex, which may explain the extraordinarily long correlation length of the streamwise momentum (cf. Townsend<sup>1</sup> for a discussion of the correlation tails). The grouping of the vortices also explains the occurrence of multiple second-quadrant events in turbulent bursts<sup>13,14,48</sup> and the lift-up/oscillation/violent ejection sequence of events observed in a turbulent burst (cf. Robinson<sup>12</sup> for a review). Put another way, the phenomena that have been associated with turbulent bursts are merely the manifestations of the passage of a hairpin packet. The weak backward induction of the larger packets causes them to propagate upstream with respect to their surrounding environment more slowly than a smaller packet, meaning that their forward velocity with respect to the wall must be faster. The sketch shows three packets at a particular instant, but the configuration is expected to be ever changing, owing to the different velocities of propagation. The sketch should not be interpreted to imply that the packets always align in the streamwise or the vertical directions, although we shall see

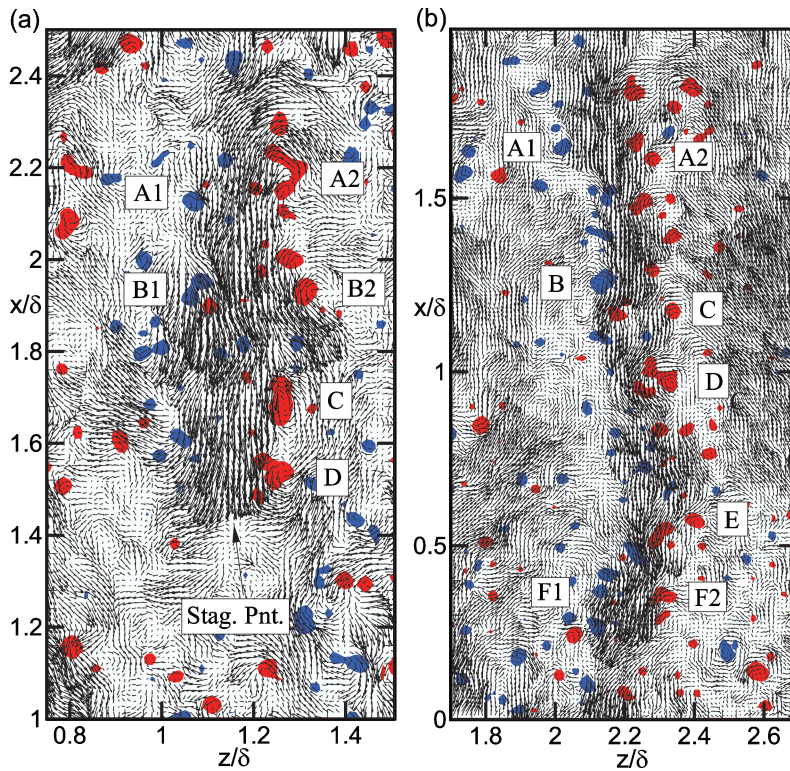


FIG. 13. (Color) Long streaks of low-momentum fluid in streamwise-spanwise planes of boundary layer flow at  $y/\delta=0.2$  and  $Re_\theta=2216$ . The red (blue) contours represent regions of swirling strength with counterclockwise (clockwise) rotation that tend to occur to the right (left) of the low-speed streaks (from Ref. 56).

that there is a tendency for meandering streamwise alignment. Another implication of the picture in Fig. 12 is that at a given  $x$  location, the structure changes from new packets created in the vicinity of  $x$  to progressively older and larger packets created farther upstream as one traverses the thickness of the boundary layer from the wall to its outer edge. Hence, the uniform momentum zones are like geographic strata, and the variations in  $y$  depend on the upstream history of the flow, which is important in flows that are developing and/or nonequilibrium.

Disturbances large enough to initiate a packet of hairpins could come from any agency that would cause a low-momentum ejection. Small bumps on the wall, disturbances from other hairpins and interactions of eddies, or upstream disturbances from the region of transition are possible sources. Of particular interest is the possibility that large hairpin packets create smaller hairpins so that smaller, nearer-wall packets have a phase relationship to larger packets. As noted earlier, the small, tertiary hairpin formed between the primary and secondary hairpins in Fig. 8 could be viewed as the start of a new packet within the environment of a larger packet. But, as yet there is no definitive determination of the processes by which packets might trigger new packets to form a pattern. All we know is that in fully turbulent flow, something(s) trigger packets continuously and in large numbers.

Low-speed streaks in the buffer layer play a crucial role in determining skin friction and producing turbulent kinetic energy and vorticity because they are the dominant mechanism in the region where most of the change of mean velocity occurs at low Reynolds number. For example, the velocity change in the region where hairpins dominate, i.e., from the top of the buffer layer to the free stream (or centerline),

does not exceed the velocity change from the wall to the top of the buffer layer until  $Re_\tau$  exceeds 5000, approximately. Consequently, many studies have focused attention on the buffer layer streaks and the associated quasistreamwise vortices<sup>29,49</sup> (cf. Refs. 50–53 and many others). The origin of the buffer layer streaks and the explanation for their mean spacing have been sought through various means, including stability analyses<sup>54,55</sup> and models in which quasistreamwise vortices (or streaks) regenerate new vortices.<sup>52,53</sup> Low-speed streaks occur in the logarithmic layer, but above the buffer layer hairpin packets also play a role in forming them.<sup>35,56</sup> Figure 13 presents samples of streaks in a plane 400 viscous length scales above the wall of a boundary layer having von Karman number  $\delta^+=2000$ , i.e., just above the logarithmic layer. The colored contours indicate swirling strength signed by the sign of the wall-normal vorticity. They correspond to legs of hairpins passing through the plane. The picture is consistent with the idea that the low-speed streak is caused by coherent vortex induction. The streamwise length, about 2000–3000 viscous units, is comparable to the length of a bulge at this Reynolds number. At this height, the heads of the hairpins replace the quasistreamwise vortices as the source of low momentum.

While low-speed streaks are often explained in terms of quasistreamwise vortices lifting slow fluid away from the wall, it is not clear how the quasistreamwise legs of hairpins could produce long streaks, because individual hairpins are relatively short. After inferring the short streamwise extent of hairpins by means of conditional analyses akin to the picture shown in Fig. 4, Kim and Moin<sup>24</sup> argued, “it is very unlikely that the vortex filaments near the wall have long streamwise extent *along the wall*.” This led them to suggest that the long streaks were like the wake left by short, fast moving wall

eddies. The autogeneration mechanism offers a different explanation for the production of long streaks in which short, local disturbances grow in the streamwise direction. Individual hairpins are about  $200\text{--}400\delta_v$ , but packets are much longer and create within them zones of uniform momentum.<sup>33</sup> Five to ten hairpins in a packet would form a streak  $1000\text{--}4000\delta_v$  long, and longer packets of larger hairpins (with larger spacing) would produce yet longer low-speed streaks. The relatively short patterns of the conditional eddies found by Kim and Moin<sup>24</sup> are consistent with high correlation within an individual hairpin, and weak correlation from hairpin to hairpin in a packet, owing to fluctuations in the inter-hairpin spacing. Autogeneration can be thought of as a means of polymerizing eddies and creating long streaks by growth in  $x$ . At the same time growth occurs in  $x$  it also occurs in  $y$ . This is a mechanism for transporting low-speed streaks out of the buffer layer.

#### IV. STATISTICAL EVIDENCE FOR PACKETS

To this point, almost all of the evidence for hairpin packets has been flow visualization, albeit using quantitative velocity and vorticity fields. It is important to establish that packets contribute to the long-time-averaged statistics of wall turbulence to a measurable degree. Marusic<sup>57</sup> has shown that the extra length predicted by the packet model improves the random hairpin model<sup>20</sup> by accounting properly for the long tails on the two-point spatial correlation functions with streamwise separation. In channel flow, proper orthogonal decomposition in the  $x$ - $y$  plane produces eigenfunctions whose vector fields contain the signatures of the hairpin vortex.<sup>58</sup> Linear stochastic estimation given a strong swirling strength event produces vector patterns consistent with hairpin packets in the  $x$ - $y$  plane<sup>59,60</sup> and the  $x$ - $z$  plane.<sup>60</sup> Since proper orthogonal decomposition and linear stochastic estimation both employ the two-point correlation as input, these results show that the two-point spatial correlation tensor contains imprints of hairpin packets.<sup>61</sup>

Conditional averages given wall shear stress events of large amplitude also produce patterns having increasing height and width downstream,<sup>43</sup> not unlike the low-momentum ramps caused by packets. Like Kim and Moin,<sup>24</sup> del Alamo *et al.*<sup>43</sup> attribute the downstream region to a wake caused by flow around the wall disturbance. The autogeneration dynamics show that there is a wake in which downstream hairpins are created, but most of the packet is associated with hairpins that actually grow in sequences that propagate *upstream, not downstream*. This is further substantiated by the work in Ref. 61. More quantitatively, it has been shown<sup>35</sup> that 25% of  $-\bar{uv}$  can be associated with hairpin vortex signatures that occupy less than 4.5% of the total area. Bearing in mind that large-scale and very-large-scale motions carry over one-half of  $-\bar{uv}$ ,<sup>62</sup> the smaller hairpins must carry at least one-half of the remainder. Larger hairpins that are less readily identified by pattern extraction schemes may carry an additional fraction, although it must be allowed that hairpins, LSMs, and VLSMs may not be the only structures contributing to Reynolds shear stress.

The growth of hairpins in packets is consistent with

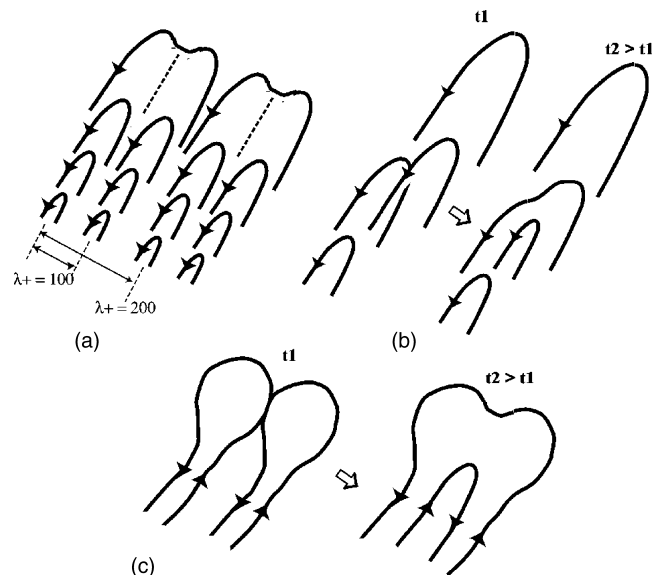


FIG. 14. Spanwise merger of hairpins by vortex reconnection of legs (from Ref. 63).

Townsend's attached eddy hypothesis, in which the sizes of the eddies are proportional to their distance from the wall.<sup>1</sup> Growth occurs in the spanwise direction and the wall-normal direction simultaneously. With increasing distance from the wall, the width of the low-speed streaks and the spacing of the hairpin legs found in conditionally averaged fields increases in close proportion to  $y$ .<sup>56</sup> This sort of growth implies self-similar structure consistent with logarithmic velocity variation, provided there is no length scale other than  $y$ . However, it also implies that the hairpins must ultimately grow so large in the spanwise direction as to encounter adjacent hairpins. When this happens, various vortex reconnection events are possible,<sup>63</sup> depending upon the shapes of the hairpins and their relative positions at the time of encounter, cf. Fig. 14. In general, the legs cut and connect so as to form wider hairpins, Fig. 14(a), or a wider hairpin plus a remainder hairpin that has the same sense of vorticity as the original hairpins, Fig. 14(b), or a wider hairpin plus a smaller hairpin with opposite sense, Fig. 14(c). Thus, the length scale can grow smoothly for a time, and then grow abruptly, then smoothly again. Evidence for abrupt growth can be found in the pattern in Fig. 10, in patterns in the plane parallel to the wall,<sup>56</sup> and in simulations of hairpin encounters.<sup>31</sup> Evidence for low-speed streaks above the logarithmic layer can be found in laboratory measurements,<sup>33,35,56,60</sup> large eddy simulations,<sup>64</sup> and the atmospheric boundary layer.<sup>46,65</sup>

#### V. LARGE SCALES OF MOTION

The hairpin packets extend beyond the logarithmic layer, and in some instances they clearly grow to the edge of the boundary layer, suggesting that at least some of the bulges may be large hairpin packets. However, there are a number of considerations that argue against growing packets being the only mechanism for turbulence production, transport, and scale growth in wall turbulence, especially in the outer half of the layer. First, linear growth of the mixing length is

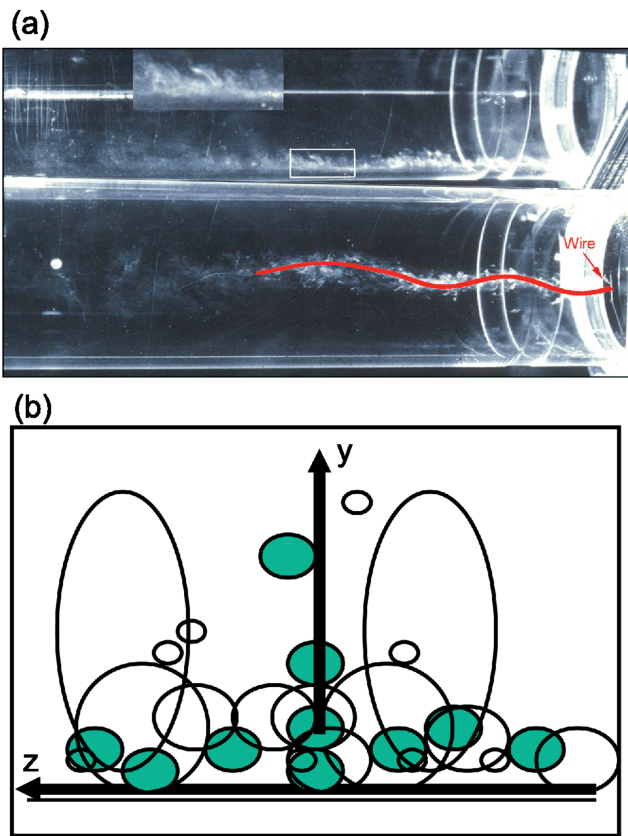


FIG. 15. (Color) (a) Visualization of multiscale motion in pipe flow using smoke injected at  $y/R=0.05$ ; (bottom) large-scale low-speed streak in the streamwise-spanwise plane; (top) view of the streamwise-wall-normal plane; (inset) expanded view of hairpins in the low-speed streak (from Ref. 62). (b) Sketch of small scales clustered between spanwise wall flows from larger-scale eddies.

known to saturate at about one-half  $\delta_0$  and become nearly constant, thereafter. Second, growth from small to large scale opposes the classical Kolmogorov energy cascade concept, which is clearly supported at sufficiently high Reynolds number by spectral data showing energy transfer from large to small. Thus, one must make allowance for a mechanism that produces large-scale kinetic energy. Third, it is known that very large-scale motions (defined in Ref. 62 to be scales longer than the longest large-scale motions, approximately  $3\delta_0$ ) carry substantial kinetic energy and Reynolds shear stress.<sup>62,66–69</sup> Figure 15(a) shows smoke-wire visualization of large-scale motions in pipe flow, and it is likely that the VLSM wavelengths in the time-series data arise from similar spatial structures. It has been suggested that the very long fluctuations in hot-wire signals are the consequence of alignment of bulges into very large-scale motions.<sup>62,67</sup> This may explain the long-wavelength oscillations, but it does not explain the mechanism by which the bulges might organize into streaks.

There is a growing body of evidence that exact coherent motions in the form of very long wavelength traveling waves exist at transitional Reynolds numbers.<sup>70–73</sup> It is interesting to speculate that motions persist into the fully turbulent regime, at least in a form that is not too strongly modified by the presence of smaller scale turbulence. For example, recent

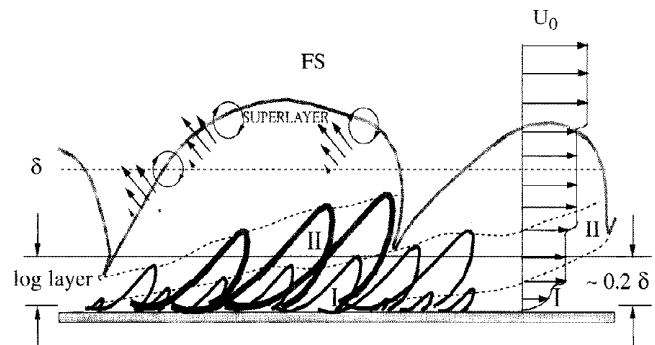


FIG. 16. Summary sketch of the organization of hairpins and packets in a boundary layer. Hairpin packets are most common in the lower half of the boundary layer, especially the logarithmic layer, creating uniform momentum zones in layers. They sometimes extend to the edge of the boundary layer and the largest ones may be the source of turbulent bulges. Detached, smaller-scale hairpin vortices can be created by shear at the turbulent-nonturbulent interface and possibly within the bulk of the layer.

stability analysis<sup>55</sup> demonstrates algebraic instability on very long wavelength when the base flow is a mean turbulent profile. Also, recent results from simulation show that at low but turbulent Reynolds numbers, the  $\delta_0$ -scale streamwise vortices and the near-wall vortices are related to one another. One interpretation is that the spanwise flows of the large scales sweep the near-wall small-scale vortices into clusters in the vicinity of the stagnation points between adjacent large-scale vortices,<sup>74,75</sup> something like the depiction in Fig. 15(b). The higher Reynolds number visualization in Fig. 15(a) indicates small-scale clustering of this type. Another idea is that the large scales initiate hairpins in the regions of clustering (see Fig. 16). Whether the relationships between the patterns of large- and small-scale motions are due to self-organization, instability of very long wavelengths, or an independent large-scale motion at high Reynolds number remains an open question.

## VI. SUMMARY

Quasistreamwise vortices, hairpin vortices, and packets of hairpins are prevalent coherent structures in wall turbulence that are coherent in the sense that they have long persistence. Quasistreamwise vortices and the associated streaks of high and low momentum are most readily observed in the buffer layer, but there is mounting evidence for their occurrence in the logarithmic layer and perhaps even in the wake region. Hairpins can occur singly, but they also occur often in packets, probably due to the autogeneration mechanism that naturally spawns multiple, streamwise-organized hairpins. The hairpins are most common in the logarithmic layer and become less frequent with increasing distance from the wall, occasionally penetrating across the entire boundary layer and perhaps forming the source of turbulent bulges. The scale of the structures grows with distance from the wall.

In the logarithmic layer, the picture is generally consistent with Townsend's attached eddy hypothesis. As hairpins form, they lift the quasistreamwise vortices and create "lifted" hairpins that may appear to be "detached," depend-

ing upon the visualization method. The growth of the packets provides a mechanism to transport vorticity, low momentum, and turbulent kinetic energy from the wall. However, the transport cannot be exclusively due to the coherent structure described here, because turbulence is also produced by gradients away from the wall, and the latter production may be due to a different mechanism. Certainly, it is recognized that the very large scales of motion support a large fraction of the Reynolds stress and the turbulent kinetic energy, and the relationship between them and the hairpin packets remains to be established for fully turbulent flows.

## ACKNOWLEDGMENTS

The assistance of J. Baltzer, K. Kim, and D. O'Donnell in preparing this paper is gratefully acknowledged. Research was supported by the U. S. National Science Foundation, the Air Force Office of Scientific Research, the Office of Naval Research, and the Ira A. Fulton Endowment.

- <sup>1</sup>A. A. Townsend, *The Structure of Turbulent Shear Flow*, 2nd ed. (Cambridge University Press, Cambridge, 1976).
- <sup>2</sup>B. J. Cantwell, "Organized motion in turbulent flow," *Annu. Rev. Fluid Mech.* **13**, 457 (1981).
- <sup>3</sup>E. R. Corino and R. S. Brodkey, "A visual investigation of the wall region in turbulent flow," *J. Fluid Mech.* **37**, 1 (1969).
- <sup>4</sup>W. W. Willmarth and S. S. Lu, "Structure of the Reynolds stress near the wall," *J. Fluid Mech.* **55**, 65 (1972).
- <sup>5</sup>R. E. Falco, "Coherent motions in the outer region of turbulent boundary layers," *Phys. Fluids* **20**, 124 (1977).
- <sup>6</sup>R. F. Blackwelder and L. S. G. Kovasznay, "Time scales and correlations in a turbulent boundary layer," *Phys. Fluids* **15**, 1545 (1972).
- <sup>7</sup>G. L. Brown and A. S. W. Thomas, "Large structure in a turbulent boundary layer," *Phys. Fluids* **20**, S243 (1977).
- <sup>8</sup>L. S. G. Kovasznay, V. Kibens, and R. F. Blackwelder, "Large-scale motion in the intermittent region of a turbulent boundary layer," *J. Fluid Mech.* **41**, 238 (1970).
- <sup>9</sup>T. Theodorsen, "Mechanism of turbulence," in *Proceedings of the Mid-western Conference on Fluid Mechanics* (Ohio State University, Columbus, OH, 1952).
- <sup>10</sup>T. Theodorsen, "The structure of turbulence," in *50 Jahre Grenzschichtforschung*, edited by H. Gortler and W. Tollmein (Friedrich Vieweg & Sohn, Braunschweig, 1955).
- <sup>11</sup>S. J. Kline, W. C. Reynolds, R. A. Schraub, and P. W. Runstadler, "The structure of turbulent boundary layers," *J. Fluid Mech.* **30**, 741 (1967).
- <sup>12</sup>S. K. Robinson, "Coherent motions in the turbulent boundary layer," *Annu. Rev. Fluid Mech.* **23**, 601 (1991).
- <sup>13</sup>D. G. Bogard and W. G. Tiederman, "Burst detection with single-point velocity measurements," *J. Fluid Mech.* **162**, 389 (1986).
- <sup>14</sup>S. Tardu, "Characteristics of single and clusters of bursting events in the inner layer, Part 1: Vita events," *Exp. Fluids* **20**, 112 (1995).
- <sup>15</sup>M. R. Head and P. R. Bandyopadhyay, "New aspects of turbulent boundary-layer structure," *J. Fluid Mech.* **107**, 297 (1981).
- <sup>16</sup>P. R. Bandyopadhyay, "Large structure with a characteristic upstream interface in turbulent boundary layers," *Phys. Fluids* **23**, 2326 (1980).
- <sup>17</sup>C. R. Smith, "A synthesized model of the near-wall behavior in turbulent boundary layers," in *Proceedings of the 8th Symposium of Turbulence*, edited by J. L. Zakin and G. Patterson (University of Missouri-Rolla, Rolla, 1984).
- <sup>18</sup>C. R. Smith, J. D. A. Walker, A. H. Haidari, and U. Sobrun, "On the dynamics of near-wall turbulence," *Philos. Trans. R. Soc. London, Ser. A* **336**, 131 (1991).
- <sup>19</sup>A. E. Perry and M. S. Chong, "The mechanism of wall turbulence," *J. Fluid Mech.* **119**, 173 (1982).
- <sup>20</sup>A. E. Perry, S. Henbest, and M. S. Chong, "A theoretical and experimental study of wall turbulence," *J. Fluid Mech.* **165**, 163 (1986).
- <sup>21</sup>A. E. Perry and I. Marusic, "A wake model for the turbulence structure of boundary layers, Part 1: Extension of the attached eddy hypothesis," *J. Fluid Mech.* **298**, 361 (1995).
- <sup>22</sup>P. Moin and J. Kim, "Numerical investigation of turbulent channel flow," *J. Fluid Mech.* **118**, 341 (1982).
- <sup>23</sup>P. Moin and J. Kim, "The structure of the vorticity field in turbulent channel flow. Part 1. Analysis of instantaneous fields and statistical correlations," *J. Fluid Mech.* **155**, 441 (1985).
- <sup>24</sup>J. Kim and P. Moin, "The structure of the vorticity field in turbulent channel flow. Part 2: Study of ensemble-averaged fields," *J. Fluid Mech.* **162**, 339 (1986).
- <sup>25</sup>S. J. Kline and S. K. Robinson, "Quasi-coherent structures in the turbulent boundary layer, Part 1: Status report on a community-wide summary of the data," in *Near Wall Turbulence*, edited by S. J. Kline and N. H. Afgan (Hemisphere, Washington, DC, 1989), p. 218.
- <sup>26</sup>P. R. Spalart, "Direct simulation of a turbulent boundary layer up to  $Re_\tau = 1410$ ," *J. Fluid Mech.* **187**, 61 (1988).
- <sup>27</sup>J. Jeong, F. Hussain, W. Schoppa, and J. Kim, "Coherent structure near the wall in a turbulent channel flow," *J. Fluid Mech.* **332**, 185 (1997).
- <sup>28</sup>P. Chakraborty, S. Balachandar, and R. J. Adrian, "On the relationships between local vortex identification schemes," *J. Fluid Mech.* **535**, 189 (2005).
- <sup>29</sup>R. F. Blackwelder and H. Eckelmann, "Streamwise vortices associated with the bursting phenomenon," *J. Fluid Mech.* **94**, 577 (1979).
- <sup>30</sup>Z.-C. Liu, R. J. Adrian, and T. J. Hanratty, "High resolution measurement of turbulent structure in a channel with particle image velocimetry," *Exp. Fluids* **10**, 301 (1991).
- <sup>31</sup>R. J. Adrian and Z.-C. Liu, "Observation of vortex packets in direct numerical simulation of fully turbulent channel flow," *J. Vision* **5**, 9 (2002).
- <sup>32</sup>Y. G. Guezenec, U. Piomelli, and J. Kim, "On the shape and dynamics of wall structures in turbulent channel flow," *Phys. Fluids A* **1**, 764 (1989).
- <sup>33</sup>R. J. Adrian, C. D. Meinhart, and C. D. Tomkins, "Vortex organization in the outer region of the turbulent boundary layer," *J. Fluid Mech.* **422**, 1 (2000).
- <sup>34</sup>J. M. Wallace, R. S. Brodkey, and H. Eckelmann, "Pattern-recognized structures in bounded turbulent shear flows," *J. Fluid Mech.* **83**, 673 (1997).
- <sup>35</sup>B. Ganapathisubramani, E. K. Longmire, and I. Marusic, "Characteristics of vortex packets in turbulent boundary layers," *J. Fluid Mech.* **478**, 35 (2003).
- <sup>36</sup>J. Zhou, R. J. Adrian, and S. Balachandar, "Autogeneration of near-wall vortical structures in channel flow," *Phys. Fluids* **8**, 288 (1996).
- <sup>37</sup>J. Zhou, R. J. Adrian, S. Balachandar, and T. M. Kendall, "Mechanisms for generating coherent packets of hairpin vortices in channel flow," *J. Fluid Mech.* **387**, 353 (1999).
- <sup>38</sup>J. W. Brooke and T. J. Hanratty, "Origin of turbulent-producing eddies in a channel flow," *Phys. Fluids A* **5**, 1011 (1993).
- <sup>39</sup>B. A. Singer and R. D. Joslin, "Metamorphosis of a hairpin vortex into a young turbulent spot," *Phys. Fluids* **6**, 3724 (1994).
- <sup>40</sup>J. M. Chacin, B. J. Cantwell, and S. J. Kline, "Study of turbulent boundary layer structure using the invariants of the velocity gradient tensor," *Exp. Therm. Fluid Sci.* **13**, 308 (1996).
- <sup>41</sup>J. Kim, P. Moin, and R. Moser, "Turbulent statistics in fully developed channel flow at low Reynolds number," *J. Fluid Mech.* **177**, 133 (1987).
- <sup>42</sup>M. Tsubokura and T. Tamura, "LES study on the very large-scale structures of wall-bounded turbulence and an effect of thermal stratification," in *Statistical Theories and Computational Approaches to Turbulence*, edited by Y. Keneda and T. Gotoh (Springer, Tokyo, 2002), p. 159.
- <sup>43</sup>J. C. Del Alamo, J. Jimenez, P. Zandonade, and R. D. Moser, "Self-similar vortex clusters in the turbulent logarithmic region," *J. Fluid Mech.* **561**, 329 (2006).
- <sup>44</sup>P. MacAulay and I. P. Gartshore, "A tentative model of outer layer structure in a turbulent boundary-layer developing on a smooth wall," in *Experimental Heat Transfer, Fluid Mechanics and Thermodynamics*, edited by J. F. Keffer, R. K. Shah, and N. Ganic (Elsevier, Amsterdam, 1991).
- <sup>45</sup>S. E. Hommema and R. J. Adrian, "Packet structure of surface eddies in the atmospheric boundary layer," *Boundary-Layer Meteorol.* **106**, 147 (2003).
- <sup>46</sup>S. C. Morris, S. Stolpa, P. E. Slaboch, and J. C. Klewicki, "Near surface particle image velocimetry measurements in a transitionally rough wall atmospheric boundary layer," *J. Fluid Mech.* (to be published).
- <sup>47</sup>C. D. Meinhart and R. J. Adrian, "On the existence of uniform momentum zones in a turbulent boundary layer," *Phys. Fluids* **7**, 694 (1995).
- <sup>48</sup>T. S. Luchik and W. G. Tiederman, "Time-scale and structure of ejections and bursts in turbulent channel flows," *J. Fluid Mech.* **174**, 529 (1987).

- <sup>49</sup>C. R. Smith and S. P. Schwartz, "Observation of streamwise rotation in the near-wall region of a turbulent boundary layer," *Phys. Fluids* **26**, 641 (1983).
- <sup>50</sup>C. R. Smith and S. P. Metzler, "The characteristics of low-speed streaks in the near-wall region of a turbulent boundary layer," *J. Fluid Mech.* **129**, 27 (1983).
- <sup>51</sup>S. L. Lyons, T. J. Hanratty, and J. B. McLaughlin, "Turbulence producing eddies in viscous wall region," *AIChE J.* **35**, 1962 (1989).
- <sup>52</sup>*Self-sustaining Mechanisms of Wall Turbulence*, edited by R. L. Panton (Computational Mechanics, Southampton, UK, 1997).
- <sup>53</sup>W. Schoppa and F. Hussain, "Coherent structure generation in near-wall turbulence," *J. Fluid Mech.* **453**, 57 (2002).
- <sup>54</sup>V. G. Primak and T. Miyazaki, "Long-wave motions in turbulent shear flows," *Phys. Fluids* **6**, 3454 (1994).
- <sup>55</sup>J. C. Del Alamo and J. Jimenez, "Linear energy amplification in turbulent channels," *J. Fluid Mech.* **559**, 205 (2006).
- <sup>56</sup>C. D. Tomkins and R. J. Adrian, "Spanwise structure and scale growth in turbulent boundary layers," *J. Fluid Mech.* **490**, 37 (2003).
- <sup>57</sup>I. Marusic, "On the role of large-scale structures in wall turbulence," *Phys. Fluids* **13**, 735 (2001).
- <sup>58</sup>Z.-C. Liu, R. J. Adrian, and T. J. Hanratty, "Large-scale modes of turbulent channel flow: Transport and structure," *J. Fluid Mech.* **448**, 53 (2001).
- <sup>59</sup>K. T. Christensen and R. J. Adrian, "Statistical evidence of hairpin vortex packets in wall turbulence," *J. Fluid Mech.* **431**, 433 (2001).
- <sup>60</sup>W. T. Hambleton, N. Hutchins, and I. Marusic, "Simultaneous orthogonal-plane particle image velocimetry measurements in a turbulent boundary layer," *J. Fluid Mech.* **560**, 53 (2006).
- <sup>61</sup>B. Ganapathisubramani, N. Hutchins, W. T. Hambleton, E. K. Longmire, and I. Marusic, "Investigation of large-scale coherence in a turbulent boundary layer using two-point correlations," *J. Fluid Mech.* **524**, 57 (2005).
- <sup>62</sup>M. Guala, S. E. Hommema, and R. J. Adrian, "Large-scale and very-large-scale motions in turbulent pipe flow," *J. Fluid Mech.* **554**, 521 (2006).
- <sup>63</sup>R. J. Adrian, S. Balachandar, and Z.-C. Liu, "Spanwise growth of vortex structure in wall turbulence," *KSME Int. J.* **15**, 1741 (2001).
- <sup>64</sup>C.-L. Lin, J. C. McWilliams, C.-H. Moeng, and P. P. Sullivan, "Coherent structures and dynamics in a neutrally stratified planetary boundary layer flow," *Phys. Fluids* **8**, 2626 (1996).
- <sup>65</sup>P. Drobinski, P. Carlotti, R. K. Newsome, R. M. Banta, R. C. Foster, and J.-L. Redelsperger, "The structure of the near-neutral atmospheric surface layer," *J. Atmos. Sci.* **61**, 699 (2004).
- <sup>66</sup>H. L. Grant, "The large eddies of turbulent motion," *J. Fluid Mech.* **4**, 149 (1958).
- <sup>67</sup>K. C. Kim and R. J. Adrian, "Very large-scale motion in the outer layer," *Phys. Fluids* **11**, 417 (1999).
- <sup>68</sup>J. Jimenez, "The largest scales of turbulent wall flows," *Annual Research Briefs* (Center for Turbulence Research, Stanford University, Stanford, 1998).
- <sup>69</sup>N. Hutchins and I. Marusic, "Evidence of very long meandering structures in the logarithmic region of turbulent boundary layers," *J. Fluid Mech.* **579**, 1 (2007).
- <sup>70</sup>F. Waleffe, "Exact coherent structures in channel flow," *J. Fluid Mech.* **435**, 93 (2001).
- <sup>71</sup>H. Wedin and R. R. Kerswell, "Exact coherent structures in pipe flow: Traveling wave solutions," *J. Fluid Mech.* **508**, 333 (2004).
- <sup>72</sup>H. Faisst and B. Eckhardt, "Traveling waves in pipe flow," *Phys. Rev. Lett.* **91**, 1 (2003).
- <sup>73</sup>B. Hof, C. W. H. van Doorne, J. Westerweel, F. T. M. Nieuwstadt, H. Faisst, B. Eckhardt, H. Wedin, R. R. Kerswell, and F. Waleffe, "Experimental observations of nonlinear traveling waves in turbulent pipe flow," *Science* **305**, 1594 (2004).
- <sup>74</sup>K. Iwamoto, N. Kasagi, and Y. Suzuki, "Dynamical roles of large-scale structures in turbulent channel flow," in *Computational Mechanics, Proceedings of WCCM VI in Conjunction with APCOM'04, 5–10 September 2004, Beijing* (Tsinghua University Press, Beijing, 2004).
- <sup>75</sup>S. Toh and T. Itano, "Interaction between a large-scale structure and near-wall structures in channel flow," *J. Fluid Mech.* **524**, 249 (2005).